

## Developed endplate geometry for uniform contact pressure distribution over PEMFC active area

Mohammad M. Barzegari<sup>a,\*</sup>, M. Ghadimi<sup>a</sup>, M. Habibnia<sup>b</sup>, M. Momenifar<sup>a</sup>, K. Mohammadi<sup>a</sup>

<sup>a</sup> Fuel Cell Technology Research Laboratory, Malek Ashtar University of Technology, Fereydoonkenar, Iran

<sup>b</sup> Islamic Azad University, Jouybar Branch, Iran, Jouybar

### Article Information

Article History:

Received:

2020-01-18

Received in revised form:

2020-04-07

Accepted:

2020-04-08

### Keywords

Geometry of endplate  
Contact pressure distribution  
Membrane electrode assembly  
Finite element simulation  
Pressure measurement film

### Abstract

Contact resistance among the components of a polymer exchange membrane fuel cell (PEMFC) has a crucial effect on cell performance. The geometry of the endplate plays an essential role in the contact pressure distribution over the membrane electrode assembly (MEA) and the amount of contact resistance between plates. In this work, the effects of endplate geometry on the contact pressure distribution over the MEA have been explored through computational simulations using ABAQUS software. A new geometry for the endplate has been proposed and was then compared to flat endplates. Geometrical parameters of an endplate having a curvature (bomb-shaped endplate) were considered, and the effects of these parameters on the contact pressure distribution over the MEA were investigated. Through the simulations, a 3D model of the fuel cell was developed. The simulation results showed good performances for the designed endplate and uniform contact pressure distribution on the fuel cell active area. Finally, a single fuel cell was manufactured and assembled using the simulation parameters, and experimental tests were conducted using pressure measurement film to evaluate the design.

## 1. Introduction

Nowadays, the utilization of renewable energy sources as suitable alternatives for fossil fuels is considered as one of the most intriguing areas of research. Among

new energy sources, comparing fuel cells with other counterparts has become an interesting new area of study. One of the parameters, which plays a pivotal role in performance, is the contact resistance between the internal components of a PEMFC. This resistance raises an ohmic loss in the fuel cell. Since this raised

\*Corresponding author: Barzegari@mut.ac.ir (M.M. Barzegari)

an ohmic loss is mainly dominated by the contact resistance between the bipolar plates and GDLs, reducing the resistance can significantly improve the performance of the cell. Consequently, the ohmic resistance is directly related to the contact pressure of the components; so, one may conclude that increasing the contact pressure can enhance the performance by lowering the ohmic resistance. However, at elevated pressures the porosity and active area of GDLs will also decrease and induce negative impacts on the performance of the cell. As a result, an optimal and uniform pressure must be exerted over the GDL to reconcile the ohmic resistance and performance. Non-uniform contact pressure causes different ohmic resistances at the interfaces. Moreover, the amount of endplate deformation has a direct influence on the contact pressure distribution over the MEA.

There have been several clamping mechanism designs patented by researchers to improve the contact pressure distribution over the active area of PEMFCs. Wozniczka [1] et al. used a mechanism to secure the stack in its assembled state, it included at least one compression band circumscribing the stack in a longitudinal direction. Grot [2] invented a mechanism for the upper endplate that included two separate plates. The upper endplate contains some threaded bores for screws, the lower ends of these screws bear against the upper face of the distributor plate. Inagaki [3] designed an endplate that has two separate plates with various types of springs arranged in parallel or in series between them to distribute the tie rods load uniformly over the PEMFC stack. Wang et al. [4] invented an endplate that contains a hydraulically pressurized pocket to uniformly distribute the load of the tie rods. Yu et al. [5] designed composite endplates with a pre-curvature that uses the thermal fabrication residual stress to replace the heavy metallic endplates. Kum et al. [6] used a clamping device which includes an oblique device and a unidirectional load control plate placed on the outside of the fuel cell stack. Alizadeh et al. [7] designed a novel clamping mechanism in which each endplate is made up of two components, with the outer and inner parts playing the role of cylinder and

piston, respectively. These components are assembled to create a pneumatically pressurized pocket endplate. Alizadeh et al. [8] improved a two dimensional model that can accurately predict compression pressure distributions over the active area of the PEMFC stack. Simulation results were validated by experimental measurements using pressure measurement films. Liu et al. [9] considered the geometrical shape and the topology structure of an endplate wherein both shape and topology optimization variables are introduced. Habibnia et al. [10] theoretically and experimentally investigated the effect of various assembly parameters to achieve proper clamping pressure over the GDL. They considered the minimum clamping force, minimum endplate deformation, and complete sealant of the system. Carral et al. [11] developed a finite element model to study the mechanical state of a PEMFC stack with a variable number of cells during its assembly process. They used several mechanical and fuel cell operation criteria to characterize the quality of the assembly. Bates et al. [12] presented an exact and efficient method for modeling and studying the clamping pressure in a single cell and a 16-cell stack assembly as well as experimental validation of the 16-cell stack simulations. Montanini et al. [13] studied the effects of various clamping pressures on the contact pressure and the endplate deformation. They used pressure sensors to measure the pressure distribution. Xing et al. [14] developed a three-dimensional model to evaluate the effects of assembly clamping pressure on the GDL's porosity/permeability and conductivity of GDLs, as well as the contact resistance between the GDLs and the current collector. Chang et al. [15] experimentally studied the effect of the clamping pressure on the electrochemical performance of the fuel cell. Ge et al. [16] determined the effects of GDL compression on fuel cell performance for different types of diffusion layers under different operating conditions. The two types of GDLs studied in this experiment were carbon fiber cloth and carbon fiber paper. Lee et al. [17] employed finite element analysis to simulate a contact pressure distribution over a single cell consisting of metallic bipolar plates.

In this work, a new geometry has been proposed for the endplate of the PEMFCs and has been compared to conventional endplates. In the next step, the geometrical parameters of the presented endplate are analyzed to achieve uniform contact pressure. To study the effects of various parameters of the endplate on the contact pressure distribution over the active area of the fuel cell, 3D finite element simulations were conducted on ABAQUS software. Finally, to validate the results, a fuel cell with the optimum parameters of the endplate geometry was assembled, and experimental tests were conducted to analyze the contact pressure distribution using pressure measurement films.

## 2. Model description

ABAQUS commercial code is used to numerically investigate the contact pressure over the MEA and the electrodes. The geometry of the model is shown in Fig. 1.

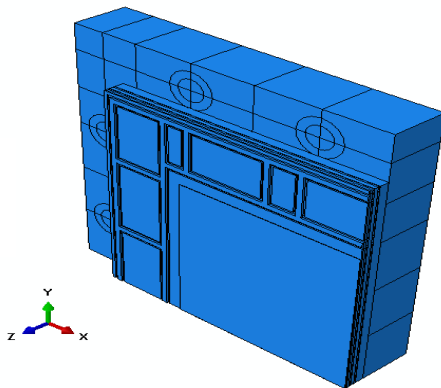


Fig. 1. Model geometry in ABAQUS software.

Due to the symmetry of the fuel cell and for computational cost purposes, the cell is divided into eight parts, and only one part is modeled. The modeled cell contains endplate, current collector, gasket, bipolar plate, GDL, and the membrane. Bolts are used to exert the clamping pressure. For simplicity purposes, compressive stresses are exerted instead of bolts in the simulation. Fig. 2 shows the positions of exerted stresses on the endplate. Exerted stress is equal to 15 MPa.

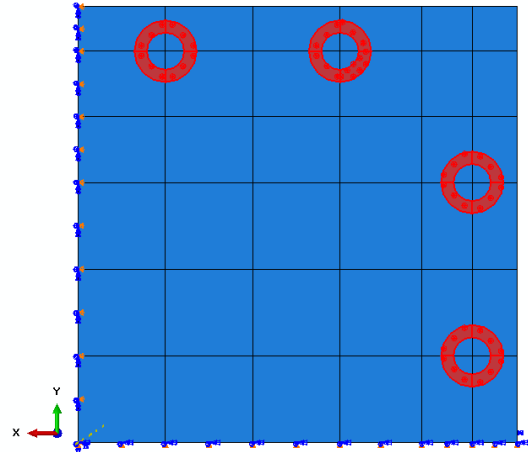


Fig. 2. The positions of bolts/compressive stresses on the endplate in the modeled cell and simulations, respectively.

The active area of MEA is equal to  $200 \times 200 \text{ mm}^2$ . The mechanical properties of the components are listed in Table 1.

Table 1. Mechanical properties of the components in the present work.

Components	Material	Young's Modulus (GPa)	Poisson's ratio	Density (kg/m <sup>3</sup> )
Endplate	Steel	209	0.3	7800
	Aluminum	70	0.3	2900
Bipolar plate	Graphite-based composite	5.1	0.25	2100
Cooling plate	Graphite-based composite	5.1	0.25	2100
Copper plate	Copper	100	0.33	8900
Gas diffusion layer	Carbon paper	0.01	0.25	400

## 3. Results and discussion

### 3.1. Effects of endplate geometry on the contact pressure distribution over MEA

Two different endplates with conventional (flat) and curved geometries are shown in Fig. 3. The PEMFCs were modeled using these two different geometries in ABAQUS software.

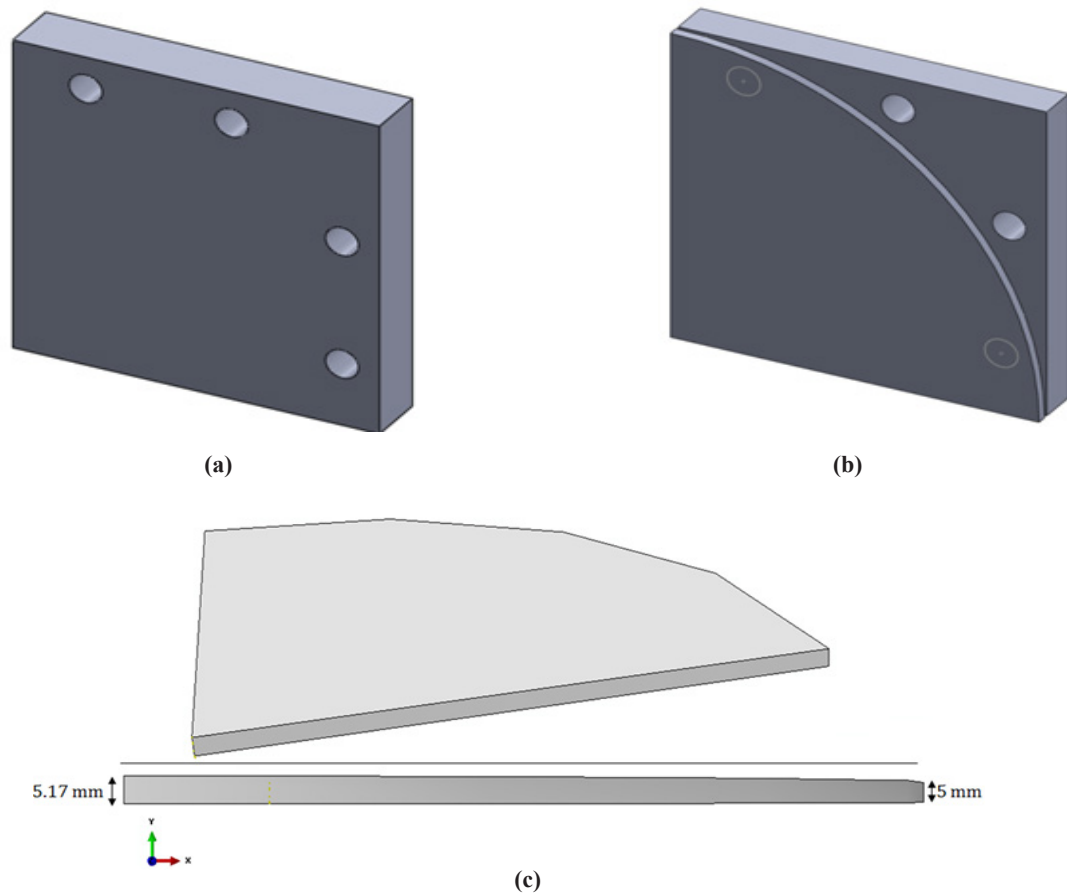


Fig. 3. Geometries of the endplates; a) conventional, b) curved c) schematic of curved endplate.

For comparison, the same parameters for design and assembly were considered in both models. The thickness of the endplate was 30 mm in both models, and steel has been selected as the material. Contact

pressure distributions over MEA for both models are shown in Fig. 4. The curvature value was considered to be 0.2 mm.

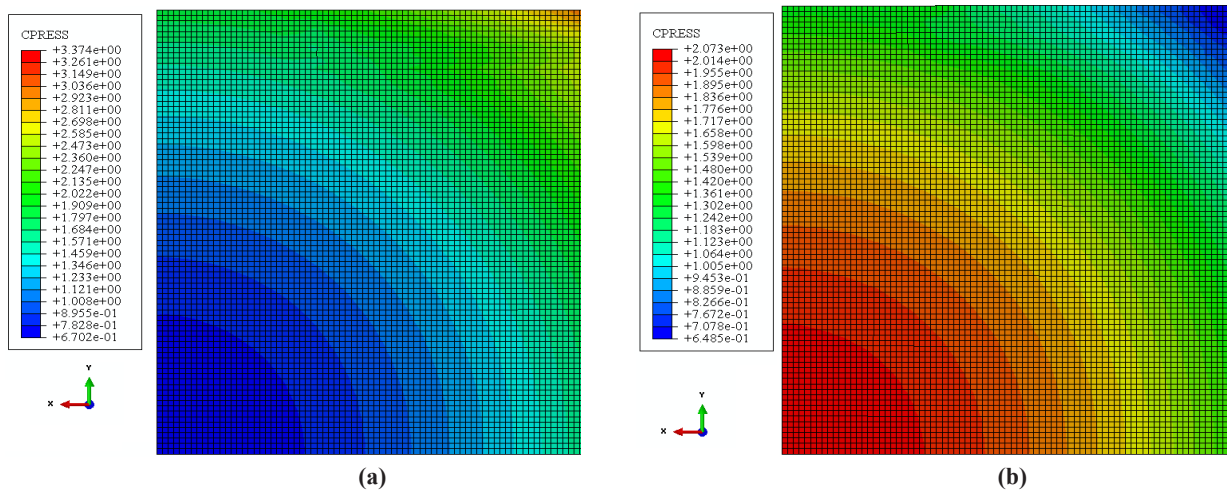


Fig. 4. Contact pressure distribution over MEA with different geometries of endplates; a) conventional, b) curved.

As it is shown in Fig. 4, the considered geometries exhibited different contact pressure distributions. In the conventional endplate, the contact pressure increased from the center towards the corner. On the other hand, in curved geometry, contact pressure

increased from the corner towards the center. To get a deeper insight, contact pressures are shown in Fig. 5 for both geometries as a function of distance from the center of MEA.

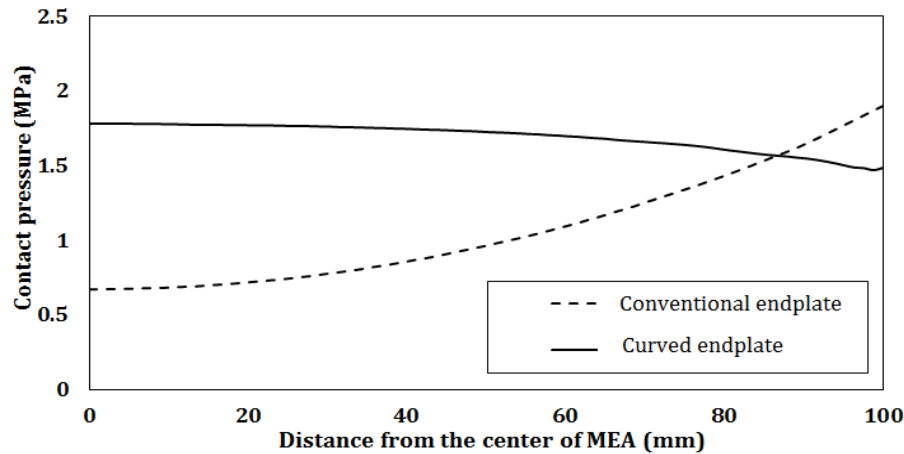


Fig. 5. Contact pressure distribution over MEA on the x-axis in two different geometries.

The mean value and the deviation from the mean value of contact pressures in both geometries

are shown in Table 2.

Table 2. Mean value and deviation from the mean value of contact pressures over MEA.

Geometry	Mean value of contact pressure (MPa)	Deviation from the mean value of contact pressure (MPa)
Conventional	0.961	0.235
Curved	1.690	0.075

As tabulated in this table, the mean value of the contact pressure increased for the case of curved endplates. Moreover, the deviation from mean value decreased, which means more uniform contact pressure over the MEA. Conventional endplates resulted in non-uniform contact pressure distribution as a result of deformation and bending created by bolt forces. The deformation in the endplate can be compensated for by using a convex plate, which is used in the geometry. To reach a uniform contact pressure over MEA, the curvature of the endplate will be discussed in the following section.

### 3.2. Effect of curvature value on the contact pressure distribution over MEA

Different curvature values were investigated for uniform contact pressure distribution in a PEMFC with a curved endplate. First, the curvatures of 0-0.25 mm with 0.05 mm steps were tried for a PEMFC. Contact pressure distribution in the x-axis is shown in Fig. 6.

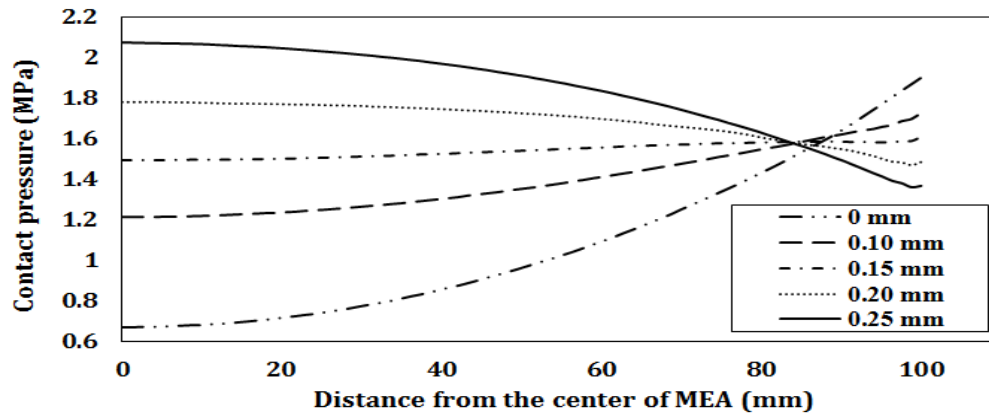


Fig. 6. Contact pressure distribution in x-direction over MEA for different curvature values.

As it is obvious in Fig. 6, more uniform contact pressure distributions were obtained by increasing the curvature value from 0 to 0.15 mm, producing higher values of contact pressure distributed over the active area. However, in higher curvature values, higher values of contact pressure were exerted over the

center of the active area rather than edges. Fig. 6 also shows that the contact pressures for the curvature of 0.15 mm to 0.20 mm are more uniform compared to other curvature values. The results obtained for the curvature values of 0.16, 0.17 and 0.18 mm are shown in Fig. 7.

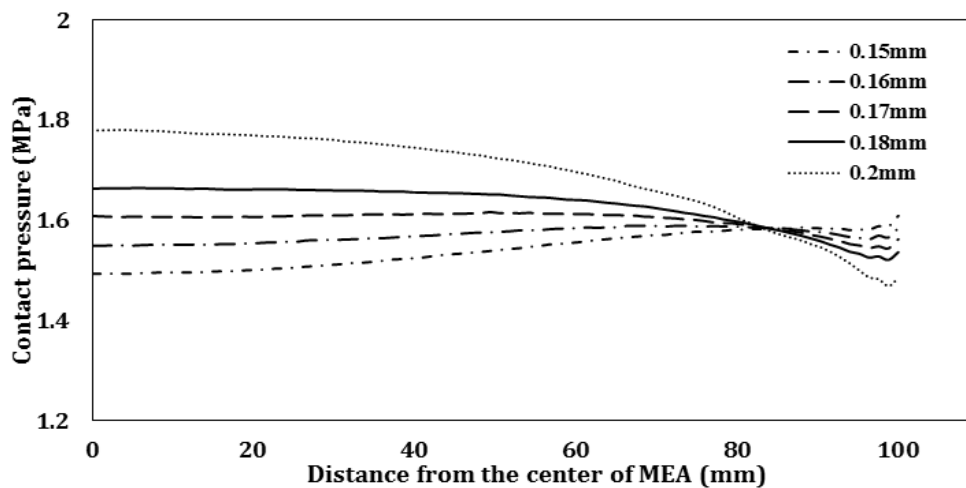


Fig. 7. Contact pressure distribution in x-axis over MEA for different curvature values.

As shown in Fig. 7, the best uniformity was obtained for endplates with curvature values of 0.16 and 0.17 mm. Table 3 lists the mean value of contact

pressure in the x-direction and its deviation as a result of different curvature values.

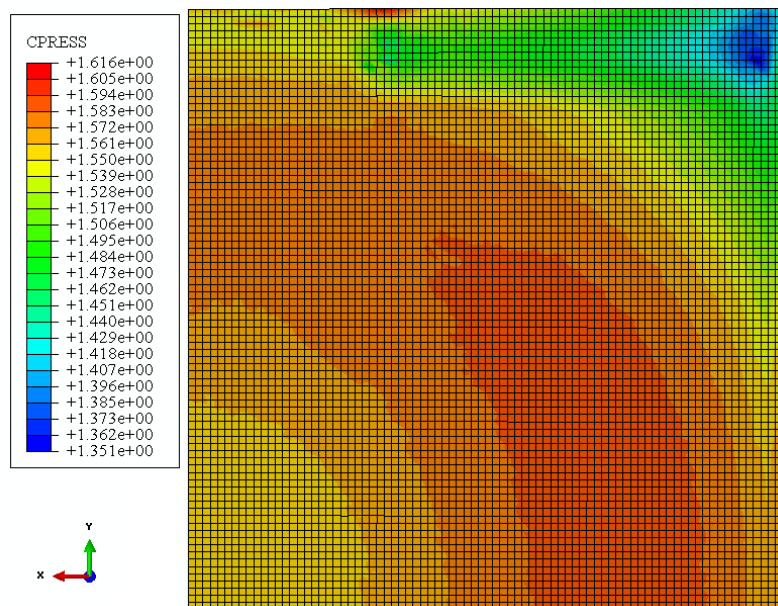
**Table 3.** Mean value of contact pressure and its deviation for endplates with different curvatures.

Curvature value (mm)	Mean value of contact pressure in the x-direction (MPa)	Deviation from the mean value of contact pressure in the x-direction (MPa)
0.10	1.39	0.131
0.15	1.54	0.031
0.16	1.57	0.012
0.17	1.60	0.014
0.18	1.63	0.033
0.20	1.69	0.075
0.25	1.84	0.184

The results demonstrate that the mean value of contact pressure increases at higher curvature values. However, the deviation decreases when the curvature value increases from 0.1 to 0.16 mm but increases for higher values of curvatures. This observation can be attributed to the fact that by increasing the curvature, the deformation of the endplates will be balanced by the clamping forces, but at higher curvatures, the contact pressure increases at the center of the MEAs. It is worth mentioning that at high curvatures, the contact pressures are higher at the center of MEAs as

compared to the corners, which lead to more deviation from the mean values.

The contact pressure distribution over MEA for the endplate with a curvature value of 0.16 mm is shown in Fig. 8. As depicted, the contact pressure distribution has improved significantly compared to conventional endplates. For comparison, the deviation decreased from 0.235 MPa to 0.012 MPa for the conventional endplates and the endplate with a curvature value of 0.16 mm, respectively.

**Fig. 8.** Contact pressure distribution over MEA for an endplate with curvature value of 0.16 mm.

### 3.3. Effect of endplate material on the contact pressure distribution over MEA

Endplates are one of the main components which affect the weight of a fuel cell. Therefore, in this paper, the effects of the endplate material (steel or aluminum)

was explored to reduce the total weight of the fuel cells. Because of the lesser rigidity of aluminum with respect to steel, aluminum plates with a thickness of 40 mm have been selected for the simulation. Fig. 9 shows the contact pressure distribution over MEA for an aluminum endplate.

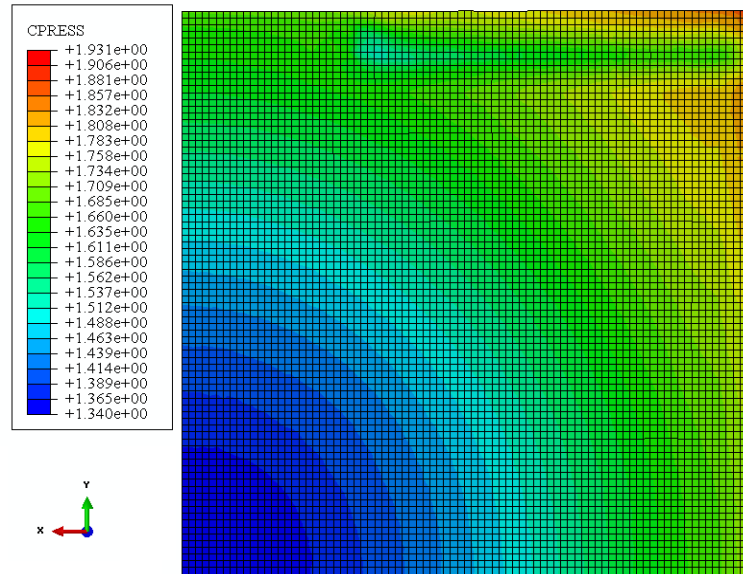


Fig. 9. Contact pressure distribution over MEA with a conventional aluminum endplate.

In the next step, the thicknesses of aluminum endplates necessary to reach a uniform contact pressure distribution are studied. Table 4 tabulates the results of the simulations in these cases. The curvature value and the clamping pressure are considered to be 0.17 mm and 15 MPa, respectively. Different curvature

values have been analyzed for this geometry, and due to the more uniform contact pressure distribution for the curvature value of 0.17 mm, this value was selected as an optimum curvature and is discussed in more details in the following section.

Table 4. Mean value and deviations of contact pressures for curved aluminum plates.

Thickness (mm)	Mean value of pressure in x-direction (MPa)	Deviation in x-direction (MPa)	Mean value of pressure in y-direction (MPa)	Deviation in y-direction (MPa)	Mean value of pressure in xy-direction (MPa)	Deviation in xy-direction (MPa)
40	1.484	0.106	1.469	0.093	1.559	0.145
43	1.550	0.017	1.538	0.008	1.518	0.040
45	1.652	0.019	1.641	0.028	1.582	0.094
50	1.769	1.108	1.762	0.115	1.603	0.247

Simulation results revealed that the contact pressure deviation in all directions has the lowest value for the endplate with a thickness of 43 mm. It should be mentioned that the thickness of the curved plate is 5 mm, and the total thickness of the endplate with this

curvature is equal to 48 mm.

Fig. 10 shows the contact pressure distribution over MEA with an aluminum endplate. It can be seen that the uniformity of contact pressure distribution improved significantly in this case.

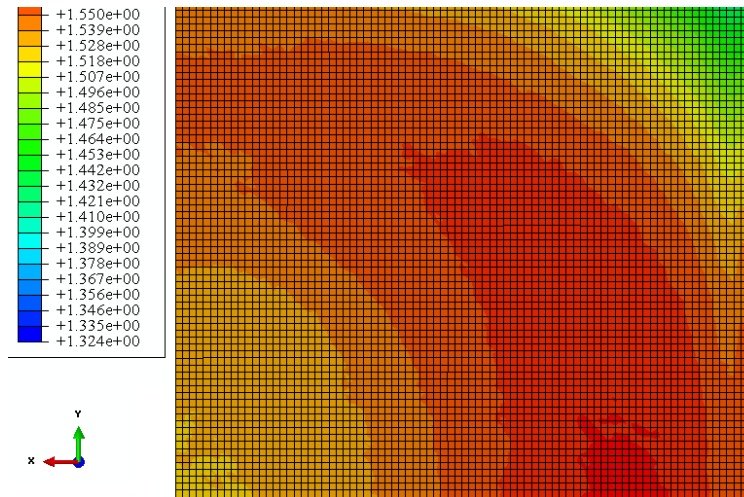


Fig. 10. Contact pressure distribution over MEA for the curved aluminum endplate.

To corroborate the results, contact pressure distributions for different thicknesses of the endplate in the x-direction are shown in Fig. 11. The distribution of Fig. 11 shows that the best uniformity was obtained

for a thickness of 43 mm and curvature of 0.17 mm. It is worth mentioning that the utilization of aluminum endplates leads to a 50 % reduction of the total weight of the endplates.

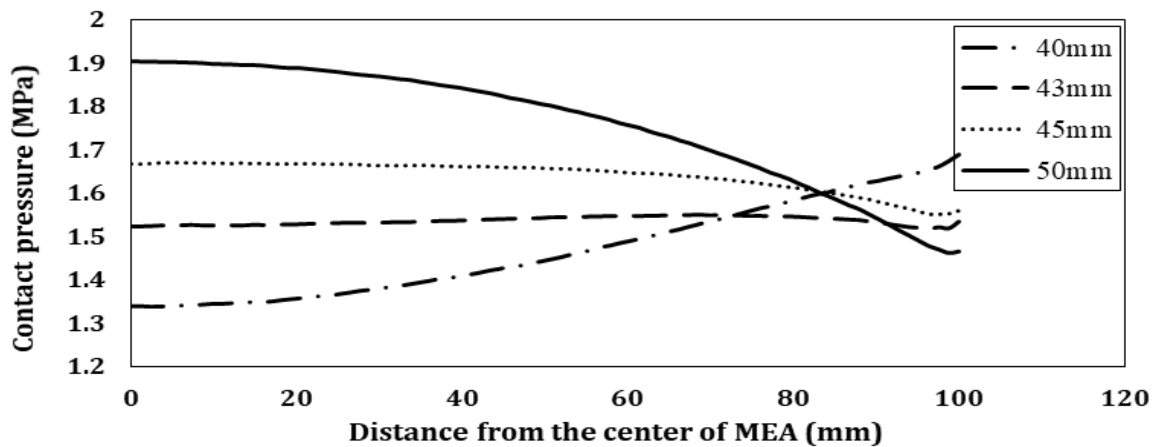
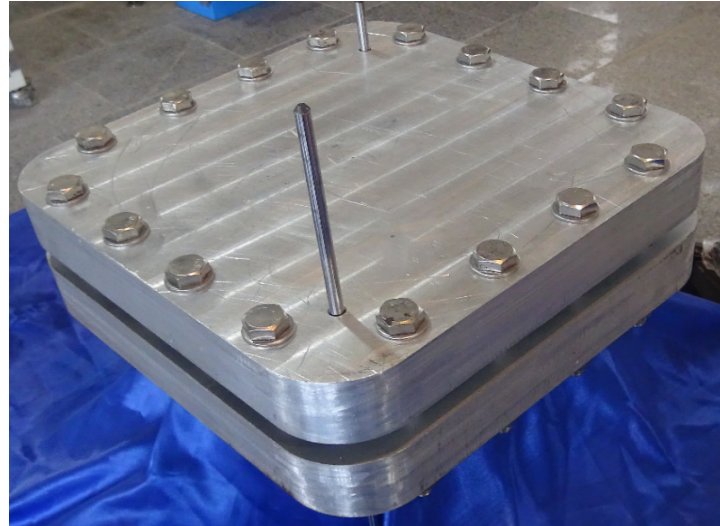


Fig. 11. Contact pressure distribution for curved aluminum endplates in the x-direction as a function of plate thickness.

### 3.4. Experimental tests

Based on the results of the finite element simulation,

a PEMFC was designed and assembled using aluminum endplate with a curvature value of 0.17 mm. Fig. 12 shows the assembled PEM fuel cell.



**Fig. 12.** PEMFC with curved aluminum endplates.

Pressure measurement films were utilized to investigate the contact pressure distribution over the active area of the MEA. The film was placed between two GDLs as shown in Fig. 13. Pressure measurement films were provided by FujiFilm Company in this

work. These films contain microcapsules of color formers which release on the film when pressure is applied. There is a direct relation between the density of the colors on the pressure films and the value of the applied pressure.

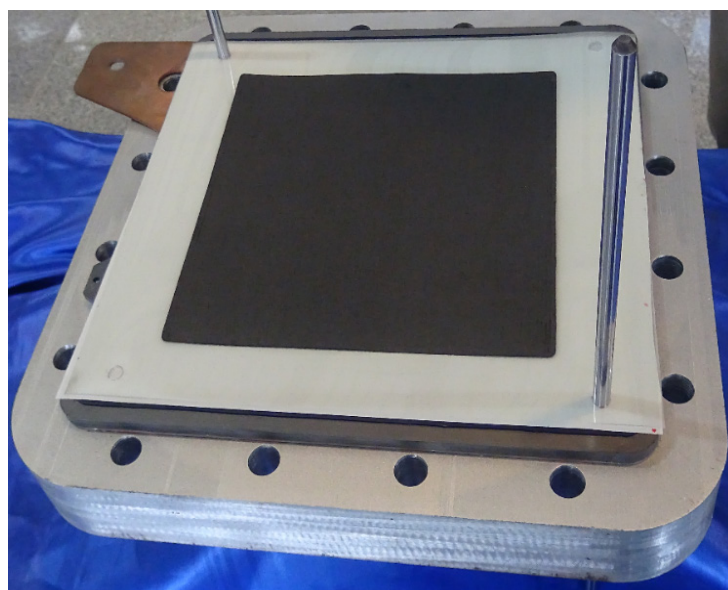


**Fig. 13.** Location of pressure measurement film in the cell.

After assembling the PEMFC components, 16 bolts were used to exert sufficient clamping pressure. The amount of torque was selected to be 13 N.m. A digital torque-meter was used to exert the exact amount of torque. The contact pressure distributions over the MEA for the (a) PEMFC equipped with the proposed curved endplate (with optimum parameters) and (b) conventional steel endplate with the thickness of

50 mm are illustrated in Fig. 14. As can be seen from this figure, the contact pressure significantly increased in the corners of the active area of the fuel cell equipped with the conventional endplate in comparison to the center, this is due to the exerted forces of the bolts. Moreover, a relatively uniform contact distribution can be observed for the fuel cell equipped with the proposed curved endplate.

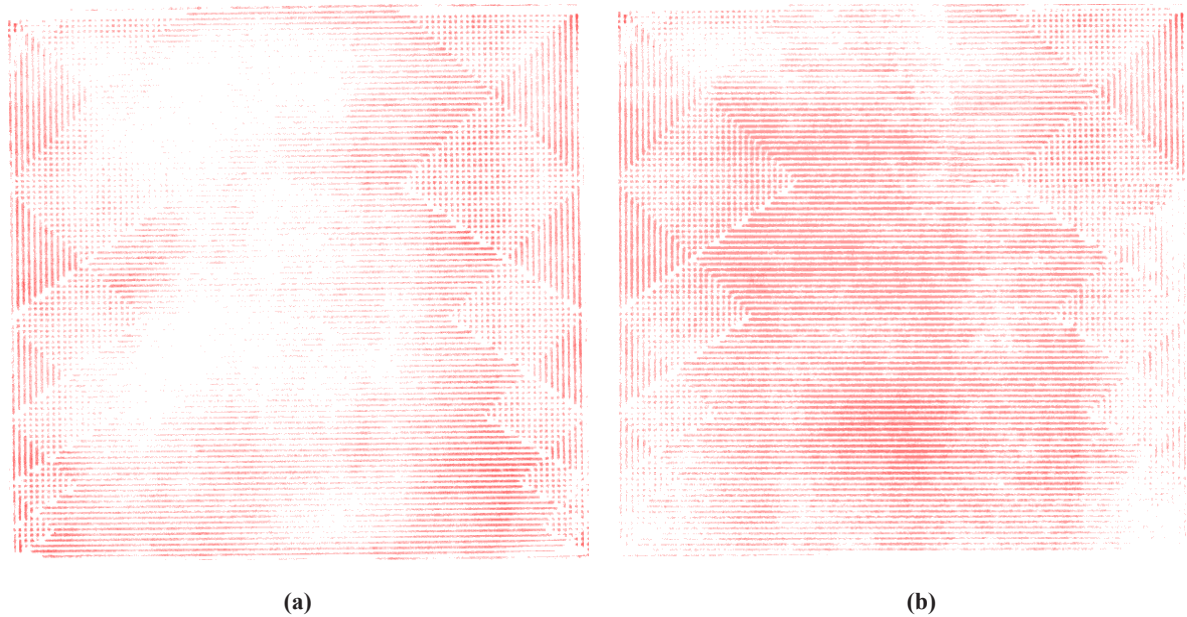


Fig. 14. The contact pressure distribution over the MEA of the PEMFC with (a) conventional endplate (b) curved endplate.

#### 4. Conclusion

In this research, a developed geometry for the endplate of PEMFCs is proposed and investigated. First, the proposed geometry was compared to conventional endplates. The simulation results revealed that in constant clamping pressure, the mean value of the contact pressure increased in the proposed model and the deviation from the mean value significantly decreased. Next, the geometrical parameters of the curved endplate were investigated to reach a uniform contact pressure distribution. The optimum geometry was obtained using finite element simulation. The simulation results showed that the most uniform contact pressure distribution could be obtained using aluminum endplate with a curvature of 0.17 mm and

a thickness of 43 mm. This geometry results in the contact pressure mean value of 1.55 MPa and deviation of 0.017 MPa. Finally, to validate the simulation results, a PEMFC was designed and assembled using the proposed endplate, and the uniformity of the contact pressure distribution was confirmed using pressure measurement films. In addition to the obtained uniform contact pressure distribution, the total weight of the proposed endplates decreased by about 50 % in comparison to conventional endplates.

#### References

- [1] Wozniczka B, Fletcher NJ, Gibb PR. Electrochemical fuel cell stack with compression bands. Google Patents; 1998.

- [2] Grot SA. Fuel cell stack compression method and apparatus. Google Patents; 2002.
- [3] Inagaki T. Fuel cell stack. Google Patents; 2010.
- [4] Wang X, Song Y, Zhang B. Experimental study on clamping pressure distribution in PEM fuel cells. *Journal of Power Sources*. 2008;179:305-9.
- [5] Yu HN, Kim SS, Do Suh J. Composite endplates with pre-curvature for PEMFC (polymer electrolyte membrane fuel cell). *Composite Structures*. 2010;92:1498-503.
- [6] Kum YB, Kim SH, Yang YC, Lee SH, Do Suh J, Yim CH, et al. Fuel cell stack clamping device. Google Patents; 2010.
- [7] Alizadeh E, Ghadimi M, Barzegari M, Momenifar M, Saadat S. Development of contact pressure distribution of PEM fuel cell's MEA using novel clamping mechanism. *Energy*. 2017;131:92-7.
- [8] Alizadeh E, Barzegari M, Momenifar M, Ghadimi M, Saadat S. Investigation of contact pressure distribution over the active area of PEM fuel cell stack. *International Journal of Hydrogen Energy*. 2016;41:3062-71.
- [9] Liu B, Wei M, Ma G, Zhang W, Wu C. Stepwise optimization of endplate of fuel cell stack assembled by steel belts. *International Journal of Hydrogen Energy*. 2016;41:2911-8.
- [10] Habibnia M, Shakeri M, Nourouzi S. Determination of the effective parameters on the fuel cell efficiency, based on sealing behavior of the system. *International Journal of Hydrogen Energy*. 2016;41:18147-56.
- [11] Carral C, Mele P. A numerical analysis of PEMFC stack assembly through a 3D finite element model. *international journal of hydrogen energy*. 2014;39:4516-30.
- [12] Bates A, Mukherjee S, Hwang S, Lee SC, Kwon O, Choi GH, et al. Simulation and experimental analysis of the clamping pressure distribution in a PEM fuel cell stack. *International journal of hydrogen energy*. 2013;38:6481-93.
- [13] Montanini R, Squadrito G, Giacoppo G. Measurement of the clamping pressure distribution in polymer electrolyte fuel cells using piezoresistive sensor arrays and digital image correlation techniques. *Journal of Power Sources*. 2011;196:8484-93.
- [14] Xing XQ, Lum KW, Poh HJ, Wu YL. Optimization of assembly clamping pressure on performance of proton-exchange membrane fuel cells. *Journal of Power Sources*. 2010;195:62-8.
- [15] Chang W, Hwang J, Weng F, Chan S. Effect of clamping pressure on the performance of a PEM fuel cell. *Journal of Power Sources*. 2007;166:149-54.
- [16] Ge J, Higier A, Liu H. Effect of gas diffusion layer compression on PEM fuel cell performance. *Journal of Power Sources*. 2006;159:922-7.
- [17] Lee W-k, Ho C-H, Van Zee J, Murthy M. The effects of compression and gas diffusion layers on the performance of a PEM fuel cell. *Journal of power sources*. 1999;84:45-51.